A Pseudoatom in a Cage: Trimetallofullerene $Y_3@C_{80}$ Mimics $Y_3N@C_{80}$ with Nitrogen Substituted by a Pseudoatom

Alexey A. Popov,[†,‡,*] Lin Zhang,[†] and Lothar Dunsch[†,*]

[†]Department of Electrochemistry and Conducting Polymers, Leibniz-Institute for Solid State and Materials Research, D-01171 Dresden, Germany, and [‡]Chemistry Department, Moscow State University, Moscow 119992, Russia

ABSTRACT Y_3C_{80} obtained in the synthesis of nitride clusterfullerenes $Y_3N@C_{2n}$ ($2n = 80-88$) by the reactive atmosphere method is found to be a genuine trimetallofullerene, $Y_3@C_{80}$, with low ionization potential and divalent state of yttrium atoms. DFT studies of the electronic structure of $Y_3@C_{80}$ show that this molecule mimics $Y_3N@C_{80}$ with the pseudoatom (PA) instead of the nitrogen atom. Topology analysis of the electron density and electron localization function show that yttrium atoms form Y—PA bonds rather than direct Y—Y bonds. Molecular dynamics simulations show that the Y_3PA cluster is as rigid as Y_3N and rotates inside the fullerene cage as a single entity.

KEYWORDS: endohedral metallofullerene · non-nuclear attractor · pseudoatom · electron localization function · topological analysis

The class of fullerenes that have atoms, ions, or clusters in their inner space is referred to as endohedral fullerenes.[1,2] Importantly, most of the species found in endohedral fullerenes are unstable in the separate form and can be stabilized only inside the fullerene cage. Encapsulated clusters range in size and can comprise up to the seven atoms (as in $Sc_4O_3@C_{80}$[3,4]). However, the high content of a metal in endohedral metallofullerenes (EMFs) can be achieved only in the form of clusters with nonmetals (such as nitrogen in $M_3N@C_{2n}$,[5−13] CH in $Sc_3CH@C_{80}$,[14] carbide unit in $M_{2,3}C_2@C_{2n}$,[15−20] or oxygen in $Sc_4O_{2,3}@C_{80}$[3]). Well-characterized conventional EMFs are limited to molecules containing one or two metal atoms. Though a larger number of encapsulated metal atoms have been reported, their characterization is mostly limited to mass spectrometry data, and there has been no evidence showing that the isolated species with three metal atoms, such as $Er_3@C_{74}$,[21] $Tb_3@C_{80}$,[22] or $Dy_3@C_{98}$,[23] are conventional trimetallofullerenes. Moreover, the EMF long thought to be a trimetallofullerene, $Sc_3@C_{82}$,[24] has been recently proved to be a carbide clusterfullerene $Sc_3C_2@C_{80}$.[18] Thus, the question whether EMFs can encapsulate three metal atoms in the form of the trimetallic cluster, in which metal−metal interactions are not mediated by the nonmetal, is still an open matter. In our studies on the synthesis of EMFs by the "reactive gas atmosphere"[8] method, we have systematically detected the species $M_3@C_{80}^+$ (M = Y, Dy, Sc) in the positive-mode LDI mass spectra of the raw fullerene extracts (Figure 1). At the same time, these species were not found in the negative mode, and our efforts to isolate these compounds have not been successful up to date presumably because of the low yield and stability of these species. In this work, we describe a tri-yttrium endohedral fullerene and employ DFT calculations to show that M_3C_{80} species are genuine trimetallofullerenes, which have peculiar electronic structure with a non-nuclear maximum of the electron density (also referred to as "pseudoatom").

RESULTS AND DISCUSSION

Molecular Structure of Y_3C_{80}. It has been shown that the carbon cage isomerism in EMFs depends on the number of the electrons formally transferred from the endohedral metal atoms to the cage. A common oxidation state of Y in EMFs is 3+ as in $Y_3N@C_{80}$ or $Y_2C_2@C_{82}$. For $Y_3@C_{80}$, this would imply the huge number of nine electrons transferred to the carbon cage as well as strong Coulomb repulsion between the endohedral Y atoms in the trimetallic cluster not mediated by the negatively charged nitride or carbide species. Hence, we suggest that the 3+ state of Y in Y_3C_{80}

*Address correspondence to a.popov@ifw-dresden.de, l.dunsch@ifw-dresden.de.

Received for review October 15, 2009 and accepted January 04, 2010.

Published online January 14, 2010. 10.1021/nn901422z

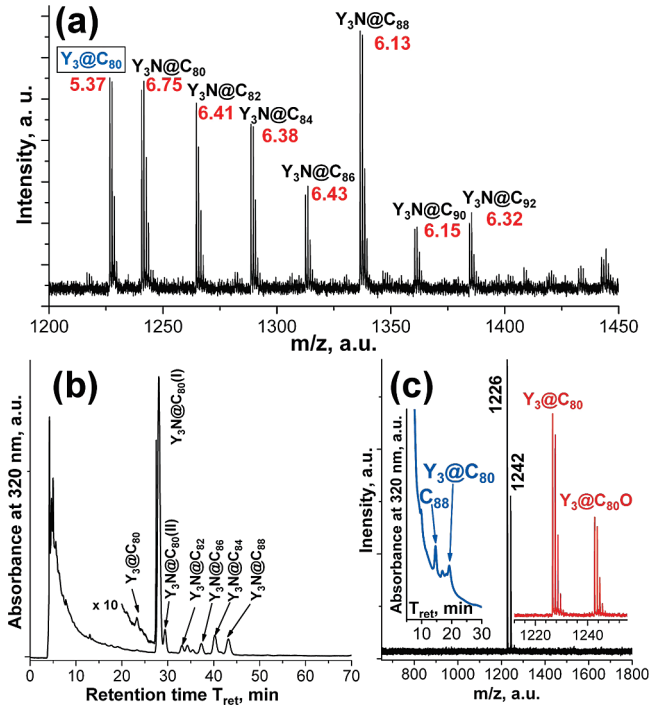

Figure 1. (a) LDI mass spectrum of the raw yttrium−EMF extract. The spectrum is measured in the positive mode, and only the range with the most intense peaks is shown; DFT-computed ionization potentials (eV) are listed in red for each compound. (b) HPLC trace of the same extract (two 4.6 × 250 mm Buckyprep columns; flow rate = 1.6 mL/min; toluene as eluent; 40 °C). (c) Mass spectrum of the fraction collected at 19 min at the Buckyprep-M column (the inset shows Buckyprep-M HPLC trace of the fraction, which was collected at 21−27 min using the Buckyprep column).

can be realized only in the carbide cluster, Y_3C_2, with $Y_3C_2@C_{78}$ as the structural model for Y_3C_{80}. Note that the Y-based carbide clusterfullerene, $Y_2C_2@C_{82}$, is one of the most abundant products in the synthesis of Y-based EMFs, while the Y_3C_2 can be obtained in a separate form.[25] As possible cage isomers of $Y_3C_2@C_{78}$, we have considered two lowest energy isomers of C_{78}^{6-}, $D_{3h}(5)$ and $C_2(22010)$ (Figure 2).[26] Alternatively, Y can adopt the formal 2+ oxidation state as in $Y_2@C_{82}$,[20] in which

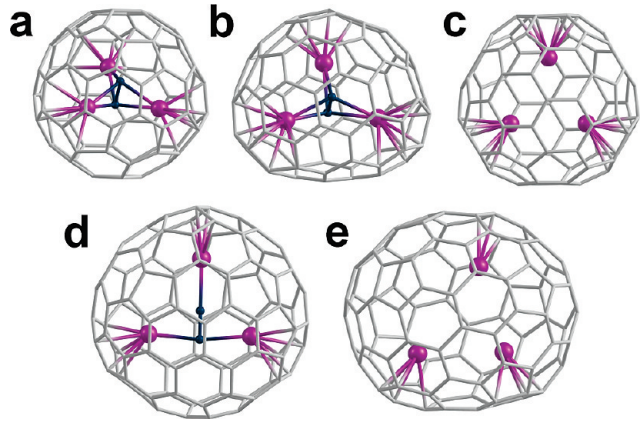

Figure 2. DFT-optimized molecular structures: (a) $Y_3C_2@C_{78}$-$D_{3h}(5)$; (b) $Y_3C_2@C_{78}$-$C_2(22010)$; (c) $Y_3@C_{80}$-$I_h(7)$; (d) $Y_3C_2@C_{96}$-$D_2(186)$; (e) $Y_3@C_{98}$-$C_2(166)$. Carbon atoms of the fullerene cage are shown in gray, carbons atoms in the carbide units are dark blue, yttrium atoms are violet.

we have recently found the covalent Y−Y bond.[27] The $(Y^{2+})_3$ cluster donates six electrons to the cage, and the most probable cage isomer is hence $I_h(7)$ as in all other EMFs with a C_{80} cage.[7,28] Kobayashi *et al.* have shown that if a Sc_3 cluster might be encapsulated in the C_{82} carbon cage then Sc atoms would adopt the 2+ oxidation state in $Sc_3@C_{82}$.[29]

DFT calculations at the PBE/TZ2P level have shown that $Y_3@C_{80}$-$I_h(7)$ is 287 and 431 kJ/mol more stable than $Y_3C_2@C_{78}$-$C_2(22010)$ and $Y_3C_2@C_{78}$-$D_{3h}(5)$ isomers, respectively. Thus, DFT shows that the lowest energy form of $Y_3@C_{80}$ is the genuine trimetallofullerene; an analogous structure can be also proposed for $Tb_3@C_{80}$ described in ref 22. In $Y_3@C_{80}$, three Y atoms are coordinated to the centers of hexagons and form a symmetric triangle with the Y−Y distance of 3.562 Å (compared to 3.656 Å in $Y_2@C_{82}$, 3.934 Å in $Y_2@C_{79}N$, and 3.566 Å in $Y_3N@C_{80}$ computed at the same level of theory). Y−C distances in the Y-coordinated hexagon span the range of 2.415−2.429 Å.

DFT calculations also showed that the high intensity of the $Y_3@C_{80}^+$ species in the positive-mode mass spectra of the raw Y-fullerene extracts can be explained by the small ionization potential (IP) of $Y_3@C_{80}$, 5.37 eV, as compared to 6.1−6.8 eV for $Y_3N@C_{2n}$ ($2n$ = 78−92) (IPs are computed as the energy difference between PBE/TZ2P-optimized structures of the neutral and cationic forms). Note that, in the $Y_3N@C_{2n}$ family, the lowest ionization potential is predicted for $Y_3N@C_{88}$, which therefore exhibits the highest intensity in the positive-mode mass spectra (while the most abundant product according to HPLC is $Y_3N@C_{80}$). This prediction agrees with cyclic voltammetry studies of $M_3N@C_{2n}$ clusterfullerenes (M = Gd, Pr, Nd, $2n$ = 80, 84, 86, 88), which showed that $M_3N@C_{88}$ has the lowest oxidation potentials.[30,31] The fact that the predicted ionization potential of $Y_3@C_{80}$ is substantially smaller even than the value for $Y_3N@C_{88}$ indicates that the actual yield of $Y_3@C_{80}$ is quite low. Besides, the ease of its oxidation is probably the main reason why current attempts to isolate these species in considerable amounts have not been successful. Indeed, we have found that $Y_3@C_{80}$ dominates in the fraction eluted at 19 min in Buckyprep-M column (Figure 1b,c); however, in the mass spectrum of this fraction, the signal of $Y_3@C_{80}$ is accompanied by the large signal of the oxide, $Y_3@C_{80}O$, which was formed during the workup procedures. Interestingly, PBE/TZ2P-computed electron affinity (EA) of $Y_3@C_{80}$, 2.61 eV, is very close to the value predicted at the same level of theory for $Y_3N@C_{80}$ (2.56 eV). Comparably low EA value of $Y_3@C_{80}$ is quite remarkable for the paramagnetic endohedral metallofullerene (for comparison, PBE/TZ2P EA of $Y@C_{82}$ is 3.64 eV). PBE/TZ2P EA values for the series of $Y_3N@C_{2n}$ ($2n$ = 78−92) molecules are also found in the range of 2.34−2.65 eV. Comparison to the IP and EA values for the experimentally available isomers of higher fullerenes C_{76}−C_{84}

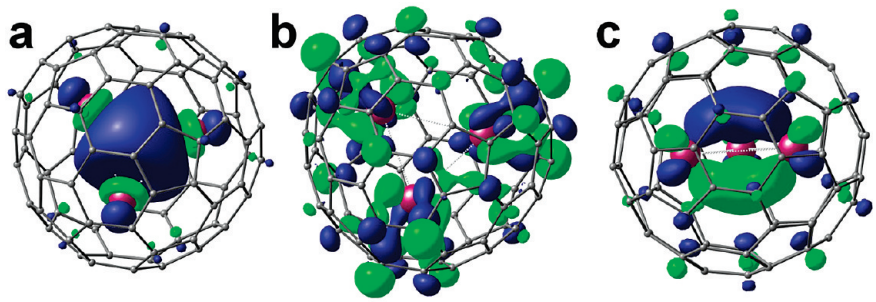

Figure 3. Molecular orbitals of $Y_3@C_{80}$: (a) HOMO; (b) SOMO; (c) LUMO+2 (this orbital resembles the p_z-like orbital of the pseudoatom).

shows that both IP and EA values of $M_3N@C_{2n}$ molecules are considerably lower than those of the empty fullerenes (see Table S1 in Supporting Information for more details); specifically, for EAs, the difference is on the order of 0.8 eV. As a result, mass spectrometric measurements of nitride clusterfullerene samples are seriously complicated even by the trace amounts of the empty fullerenes; at the same time, such problems are not encountered in the positive ion mode.

It should be noted that formation of $Y_3@C_{80}$ is somehow facilitated in the "reactive gas atmosphere" method, while these species were not observed when N_2 gas was used as the source of nitrogen.[32] At the same time, the $Y_2@C_{79}N$ reported by Dorn and co-workers[32,33] was not formed in noticeable amounts under our conditions.

In the view of the recent isolation of $Dy_3@C_{98}$,[23] we have also studied the possible isomers of $Y_3C_2@C_{96}$ and $Y_3@C_{98}$. For each fullerene, 10 lowest energy C_{2n}^{6-} cage isomers were considered,[34] and for each cage isomer, two-three conformers (different in the orientation of the internal cluster with respect to the cage) were computed. These calculations have shown that the most stable structures of $Y_3C_2@C_{96}$ and $Y_3@C_{98}$ are based on the C_{96}-D_2(186) and C_{98}-C_2(166) cage isomers, respectively, and that the former is 50 kJ/mol lower in energy. This energy difference is not so large to definitively rule out conventional trimetallic EMFs $M_3@C_{98}$, but formation of the carbide clusterfullerenes $M_3C_2@C_{96}$ appears to be more likely in this case.

Electronic Structure of $Y_3@C_{80}$. Since Y atoms in $Y_3@C_{80}$ are in the formal 2+ oxidation state, a complex Y−Y bonding situation can be expected in this molecule. Figure 3a,b shows HOMO and SOMO orbitals of $Y_3@C_{80}$. The highest two-fold occupied orbital is totally symmetric and is predominantly formed by the combination of 5s atomic orbitals of Y atoms. Similar orbitals are known for metal clusters, and their description as "interstitial" orbitals was given by Goddard *et al.*[35] SOMO of $Y_3@C_{80}$ is mainly localized on the cage, with the Y contribution being relatively small.

Further details of the bonding in $Y_3@C_{80}$ are obtained from the topological analysis of the electronic density using quantum theory of atoms-in-molecule[36] (QTAIM) and electron localization function[37−39] (ELF) approaches. A molecular graph of $Y_3@C_{80}$ is shown in Figure 4a. According to QTAIM, each Y atom bears the charge of +1.35 (the same value is found in $Y_2@C_{82}$[27]) and exhibits six bond paths to the carbon atoms of the nearest hexagon. The δ(Y,C) delocalization indices (*i.e.*, Y−C bond orders) for the Y-coordinated hexagon span the range of 0.18−0.21. Y-cage bonding pattern in $Y_3@C_{80}$ is similar to that found in $Y_3N@C_{80}$ (Figure 4b), which also exhibits six bond paths to the carbon cage for each Y atom. However, the charge of the Y atom in $Y_3N@C_{80}$ is significantly larger (+1.90), while δ(Y,C) de-

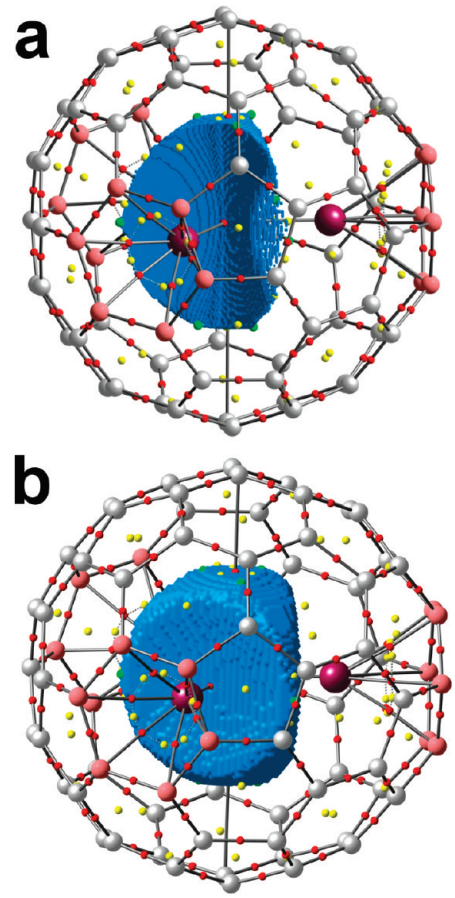

Figure 4. Molecular graphs of $Y_3@C_{80}$ (a) and $Y_3N@C_{80}$ (b). Yttrium atoms are violet, carbon atoms are gray or pink (if bonded to Y); bond, ring, and cage critical points are red, yellow, and green, respectively. Bader volumes of the nonnuclear attractor in $Y_3@C_{80}$ and the nitrogen atom in $Y_3N@C_{80}$ are shown in blue.

localization indices are smaller (0.15−0.17). The total number of the electron pairs shared between each Y atom and the cage, δ(Y,cage), is 2.46 (compared to 2.35 in $Y_2@C_{82}$ or 1.77 in $Y_3N@C_{80}$).

The similarity of the $Y_3@C_{80}$ and $Y_3N@C_{80}$ is further emphasized when the intracluster bonding is analyzed. Surprisingly, we have not found evidence for direct Y−Y bonds in $Y_3@C_{80}$. Instead, the non-nuclear attractor (NNA, *i.e.*, the maximum of the electron density also referred to as "pseudoatom") is found in the center of the molecule, and each Y atom forms a bond path to the NNA. Thus, the NNA in $Y_3@C_{80}$ mimics the nitrogen atom, and the bonding in the Y_3 cluster is similar to that in Y_3N. In fact, molecular graphs of $Y_3@C_{80}$ and $Y_3N@C_{80}$ are completely isomorphic (*i.e.*, they exhibit the same number and similar location of critical points, including the presence of BCPs between N or NNA and the cage carbon atom as well as multiple ring and cage critical points; see Figure 4). A pseudoatomic nature of the NNA can be also emphasized by the analysis of the molecular orbitals. The interstitial orbital (Figure 3a) can be understood as an s-like orbital of the pseudoatom (it is the only double-occupied orbital of the pseudoatom). Besides, we have also found a p_z-like orbital of the pseudoatom (Figure 3c) among the low-energy vacant orbitals of $Y_3@C_{80}$. However, there is certainly no quantitative correspondence between NNA and the nitrogen because the charge of NNA is only −0.19 (−0.24 if cc-pVTZ basis set is used for Y), while the charge of N in $Y_3N@C_{80}$ is −1.83. Besides, the Y−NNA bond critical points (BCPs) are located very close to the NNA, while the Y−N BCPs are approximately between the atoms. The Bader volume of NNA is also much smaller (Figure 4) than that of the nitrogen. Therefore, the NNA can be considered as a weakly charged "soft and small" ion. Finally, in spite of the absence of Y−Y bond paths, δ(Y,Y) indices in $Y_3@C_{80}$ are rather large, 0.29, while δ(Y,NNA) values are relatively small, 0.08, which is not surprising taking into account small volume and electron population of the NNA. In $Y_3N@C_{80}$, δ(Y,Y) indices are negligible (0.02), while δ(Y,N) indices are 0.72. The topology of the electron density in $Y_3@C_{80}$ is only slightly altered by the removal of one electron. In the $Y_3@C_{80}^+$, Bader charge of Y atoms is increased to +1.45, while the δ(Y,cage) index is 2.37. NNA population, −0.160, and δ(Y,NNA) and δ(Y,Y) values, 0.08 and 0.29, respectively, are almost identical to those in the neutral $Y_3@C_{80}$ molecule.

Pendas *et al.* have shown that the formation of NNA is possible at certain interatomic distances for almost all dimers of the first three periods.[40] However, for most elements, equilibrium distances are usually larger than those at which NNAs are formed. The notable exception is Li, and NNAs are typical for Li clusters;[41] for other alkaline metals, the equilibrium distances can be close to the values at which NNAs can exist, and their formation can be achieved at an increased pressure. In general, it was shown that the formation of NNA is more likely for the light elements, while for the heavier elements, equilibrium interatomic distances are usually much larger than those at which NNAs can be formed.[40] To our knowledge, the possibility of NNA has been discussed neither for such heavy elements as yttrium nor for fullerenes. At the same time, we should note that NNA was not found in $Y_2@C_{82}$ even when the Y−Y distance was reduced to 2.456 Å (*viz.* equilibrium distance of 3.656 Å). Thus, formation of NNAs appears to be more probable in polyatomic clusters. Our analysis shows a clear relationship between the presence of interstitial orbital and NNA, and hence NNAs can be probably found in many other metal clusters in which this option has not been considered yet.

Recently, with the use of scanning tunneling microscopy and plane-wave DFT calculations, Petek and coworkers discovered highly delocalized atom-like orbitals in C_{60} (referred to by the authors as "superatom" molecular orbitals, SAMOs).[42,43] The authors have shown that the origin of such orbitals is the exchange-correlation potential of spherical C_{60} molecule, and hence, analogous orbitals can be expected for spherical molecules of other types. The authors have also found that while in C_{60} such orbitals lay more than 3 eV above the LUMO they can be stabilized by doping the fullerene with the metal atoms, especially those with high ionization potentials. In $Cu@C_{60}$, SAMO orbital was found to be occupied. However, with stabilization of SAMOs, they have been also becoming more localized in the inner part of the carbon cage, losing their diffuse nature. One can find clear parallels between SAMOs and interstitial orbitals, discovered by Goddard *et al.* for the metal clusters.[35,44] This can be especially well seen for the tetrahedral metal clusters, in which s-like orbital localized at the center of the cluster is formed from the linear combinations of the atomic s-orbitals. We have already mentioned that the HOMO of $Y_3@C_{80}$ resembles the interstitial orbital of the Y_3 cluster. Following the results of Petek *et al.*,[43] one can expect that SAMOs of the carbon cage should be also affected by the Y_3 cluster. Moreover, it is natural to expect that the s-type SAMO of the cage can hybridize with the cluster orbitals. At the same type, low symmetry of the cluster should also break the cage symmetry, hence affecting the SAMOs and probably causing their mixing with the atom-localized orbitals. Since SAMOs cannot be fully revealed in the atomic-centered basis set, we have performed additional calculations of $Y_3@C_{80}$ molecule using plane-wave basis set. First, we have ensured that the method of theory and the code used in this work reproduce SAMOs found by Petek *et al.*[42,43] in C_{60}. In close agreement with the data from ref 42, the s-type SAMO was found 3.25 eV above the LUMO, followed by the p-type SAMOs at 3.88 eV above the LUMO. Calculations for the $Y_3@C_{80}$ revealed that the atom-localized basis set reliably describes the orbitals shown

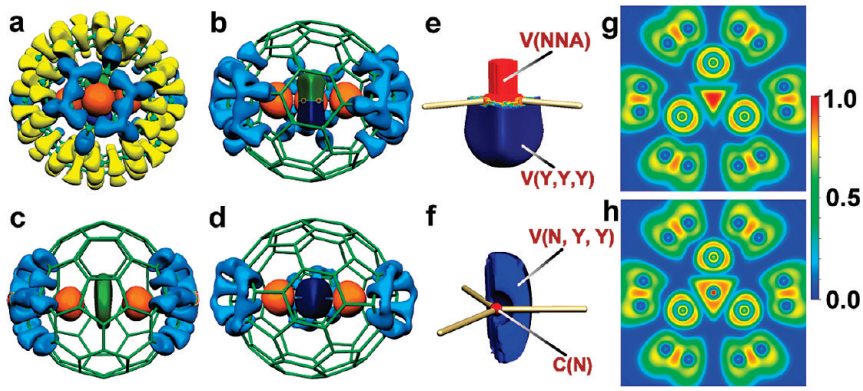

Figure 5. Spatial distribution of electron localization function (ELF): (a−d) ELF (isovalue 0.72) in $Y_3@C_{80}^+$ (a,b), $Y_2@C_{82}$ (c), and $Y_3N@C_{80}$ (d); color code for basins: yellow, V(C,C); light green, C(C); light blue, V(Y,C,C); orange, C(Y); dark blue/green, V(Y,Y,Y), V(Y,Y), and V(N,Y,Y); valence V(C,C) and core C(C) basins are not shown in b−d. (d−f) Enlarged view of ELF in the Y_3 (e) and Y_3N (f) clusters; one V(Y,Y,Y) for Y_3 and two V(N,Y,Y) basins for Y_3N are not shown. (g,h) Two-dimensional map of ELF in $Y_3@C_{80}^+$ (g) and $Y_3N@C_{80}$ (h) in the plane of the yttrium atoms. Shell structure of the N and Y atoms can be clearly seen.

in Figure 1a,b and that no new MO states are found in the energy range of the frontier orbitals. The SAMO contribution to the LUMO of $Y_3@C_{80}$ can be seen when the orbital is plotted with low isovalues, but it is clear that, just like in the case of $Cu@C_{60}$, this orbital is mostly constrained to be inside the carbon cage (hence atomic basis set is sufficient for its correct description). We have found some orbitals with the SAMO contribution in the range of 0−3 eV above the LUMO, but in all of them, the contribution of the metal-localized orbitals or the π-type cage contribution is dominating. The true SAMOs are found only at much higher energies, beyond 3 eV above the LUMO of $Y_3@C_{80}$ (see Table S3 in the Supporting Information for more details on MOs of $Y_3@C_{80}$).

One should distinguish "pseudoatomic" (or "superatomic") orbitals formed by the spherical potential (and probably modulated by the endohedral atoms or cluster, such as Y_3 cluster in $Y_3@C_{80}$) and "pseudoatoms" or "non-nuclear attractors" revealed in the topological analysis of the electron density. The orbitals are the objects in the Hilbert space, while the latter are the real-space phenomena. Furthermore, the orbitals are generated by the positive charge, while non-nuclear attractor of the electron density is the center of the negatively charged basin. Yet, there is a genetic relationship between these objects in that the s-type atomic-like orbitals have the orbital density maximum at the center of the generating potential, and when such s-orbitals are occupied, the maximum of the electron density emerges in this point.

Figure 5 shows the spatial distribution of electron localization function (ELF) in $Y_3@C_{80}^+$, $Y_2@C_{82}$, and $Y_3N@C_{80}$. Formation of the chemical bond in terms of ELF can be visualized as polysinaptic valence basins. For instance, disynaptic valence carbon−carbon basins, V(C,C), are typical for the fullerenes (see Figure 5a). Y-cage bond formation can be clearly visualized by the transformation of the valence disynaptic V(C,C) basins into the trisynaptic V(Y,C,C) basins, which are more spatially expanded than V(C,C) at the same ELF isovalue[45] (Figure 5a). Stronger Y-cage interactions in $Y_3@C_{80}$ and $Y_2@C_{82}$ compared to $Y_3N@C_{80}$ are reflected in the larger number of V(Y,C,C) basins found in these molecules (Figure 5b−d). If the presence of the NNA is not taken into account in ELF analysis, two trisynaptic V(Y,Y,Y) basins with an occupation of 0.94 *e* each are found in $Y_3@C_{80}^+$. When NNA is also considered, valence V(NNA) basin with occupation 0.19 *e* is found, while occupa-

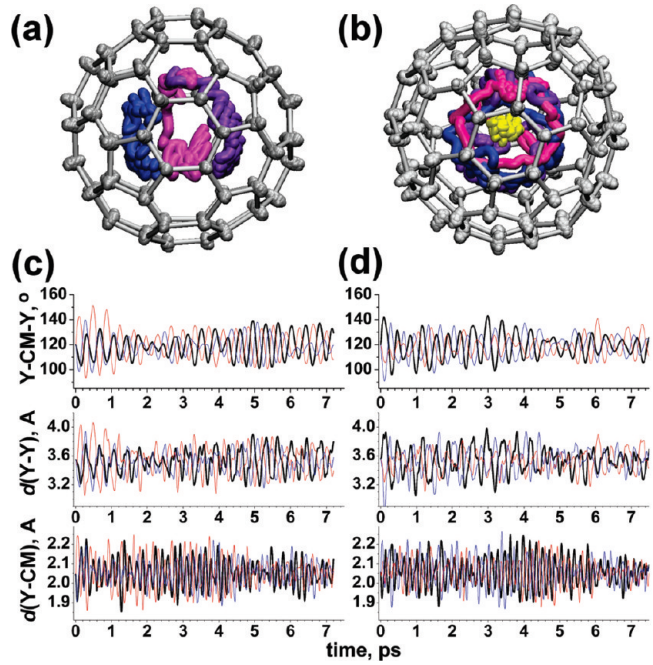

Figure 6. Molecular dynamics simulations. Trajectories of $Y_3@C_{80}^+$ (a) and $Y_3N@C_{80}$ (b) followed for 7 ps in the microcanonical ensemble after equilibration of the molecules at 300 K for 0.6 ps (carbon atoms are gray, yttrium atoms are blue, violet, and magenta, nitrogen atom is yellow; fuzzy positions of the carbon atoms are due to the vibrations of the carbon cage). (c,d) Variation of Y−CM−Y angles, Y−Y, and Y−CM distances in $Y_3@C_{80}^+$ (c) and $Y_3N@C_{80}$ (d) over the MD trajectory. All three possible parameters are shown for each item as thick black and thin red and blue curves. The scale is the same for c and d; equilibration period was 0.6 ps in each case.

tion of V(Y,Y,Y) basins is reduced to 0.84 *e*. The total occupation of these basins is close to 2, showing that they mainly originate from the density of the interstitial orbital, which is well localized in the center of the cage. In $Y_2@C_{82}$, one disynaptic V(Y,Y) basin with the occupation of 1.71 is found. For comparison, an analogous analysis of $Y_3N@C_{80}$ exhibits core nitrogen C(N) basin and three trisynaptic valence V(N,Y,Y) basins (Figure 5d,f), each occupied by 2.43 electrons. While the number of electrons in the intracluster basins is different, their shapes and spatial distribution are very similar in $Y_3@C_{80}^+$ and $Y_3N@C_{80}$. Moreover, if the number of electrons contributed by the nitrogen atom is subtracted from the total population of V(N,Y,Y) basins in $Y_3N@C_{80}$, the remaining number of 2.3 electrons is close to the total occupation of V(Y,Y,Y) and V(NNA) basins in $Y_3@C_{80}^+$. The similarity of the intracluster basin sets in $Y_3@@C_{80}^+$ and $Y_3N@C_{80}$ can be especially well seen in the ELF mapped in the plane of Y_3 atoms (Figure 5g,h). Note that the structuring of the outermost core shell of Y atoms induced by the bond formation[39] is also very similar in two molecules.

Molecular Dynamics Simulations. To study the dynamic stability of the Y_3 cluster inside the carbon cage, we have performed molecular dynamics (BOMD) simulations of $Y_3@C_{80}^+$ and $Y_3N@C_{80}$ (since our calculations have shown that the intracluster bonding situation in $Y_3@C_{80}$ and $Y_3@C_{80}^+$ is virtually the same, BOMD calculations were performed for the closed-shell cation to facilitate longer propagation time). Figure 6a,b shows snapshots of MD trajectories of the two species followed for 7 ps after equilibration at 300 K for 0.6 ps. The average temperature over the trajectory was 271 K for $Y_3@C_{80}^+$ and 297 K for $Y_3N@C_{80}$. M_3N clusters are known to rotate freely in $M_3N@C_{80}$, at least at the NMR time scale.[5,46,47] Our simulations show that, over the period of 4 ps, the Y_3N cluster accomplished rotation by almost 360° around one of its Y−N bond. Then rotation axis was switched, resulting in long curved trajectories for all Y atoms. Displacements of the nitrogen atom are also significantly larger than those of the cage carbon atoms, which is the result of the coupled cluster rotation and nitrogen-out-of-plane vibration (the latter exhibits rather large amplitude in these condition; note that, for the static $Y_3N@C_{80}$ at 0 K, PBE/TZ2P predicted frequency of this mode is only 99 cm^{-1}). The Y_3 cluster in $Y_3@C_{80}^+$ also exhibits considerable displacements over the period of 7 ps; however, displacement amplitudes are slightly smaller than in the Y_3N cluster. We propose that the stronger Y-cage bonding revealed in $Y_3@C_{80}$ by QTAIM as compared to $Y_3N@C_{80}$ results in somewhat more hindered rotation of the cluster compared to Y_3N. At the same time, smaller displacements of the Y_3 cluster can also be caused by the lower average temperature over the trajectory. In any case, displacements of the Y_3 cluster observed over 7 ps are still rather large, and hence, free rotation of the cluster is expected at the longer time scale.

To analyze the changes of the cluster structure in the course of the MD run, we have plotted selected structural parameters of the cluster as a function of time in Figure 6c,d. Following the position of the NNA in $Y_3@C_{80}^+$ along the trajectory is still too computationally demanding, and hence, we analyzed the changes of the angles between two yttrium atoms and the center of mass (CM) of the molecule as well as the deviations of the Y−CM distances. For the sake of comparison, analogous parameters are also studied for the Y_3N cluster in $Y_3N@C_{80}$. Because of the displacements of the nitrogen atom, Y−CM−Y angles and Y−CM distances are not equal to the Y−N−Y angles and Y−N distances. However, we have found that Y−CM−Y and Y−N−Y angles do correlate very well. At the same time, vibrations of the Y−N bonds in $Y_3N@C_{80}$ occur with higher frequencies and smaller amplitude variations of the Y−CM distances.

Figure 6c,d shows that, over the trajectory, the Y−CM−Y angles in both Y_3 and Y_3N clusters oscillate around 120° with the deviations barely exceeding 20°. Likewise, the Y−Y and Y−CM distances also oscillate around their equilibrium distances with the amplitudes of *ca.* 0.4 and 0.2 Å. Therefore, both clusters are rather rigid. While this result is more or less trivial for the Y_3N cluster, which has strong polar covalent Y−N bonds,[27] this is an interesting finding for the Y_3 cluster in $Y_3@C_{80}^+$. Importantly, the rigidity of the Y_3 cluster is very similar to that of the Y_3N.

In summary, we have shown that $M_3@C_{80}$-I_h(7) species are likely to be genuine trimetallofullerenes with the non-nuclear maximum of the electron density in the center of the M_3 cluster, which thus mimics the nitrogen atom in the $M_3N@C_{80}$-I_h(7) nitride clusterfullerenes. At the same time, we have shown that formation of carbide clusterfullerenes $M_3C_2@C_{96}$-D_2(186) is more likely than formation of conventional trimetallofullerenes, $M_3@C_{98}$. QTAIM analysis of $Y_3@C_{80}$ reveals that yttrium atoms are bonded to NNA, and that there are no direct Y−Y bond paths in $Y_3@C_{80}$. While further molecular dynamics simulation with longer equilibration, longer system propagation, and better temperature control are needed to provide the quantitative description of the cluster dynamics in these molecules, our present study clearly shows that the Y_3 cluster is rather rigid and tends to rotate inside the cage as a single entity, while variation of the structural parameters of the cluster over the trajectory is in the same range as found for the Y_3N cluster in the $Y_3N@C_{80}$. Thus, dynamics and electronic structure of the Y_3 cluster strongly resemble those of Y_3N. In few words, yttrium atoms do not "notice" when the nitrogen atom is removed from $Y_3N@C_{80}$ and sustain the same bonding pattern and dynamical stability in $Y_3@C_{80}$ as in the nitride clusterfullerene. Further work on the isolation of EMFs with trimetallic clusters for their further structural characterization is in progress in our group.

EXPERIMENTAL DETAILS

The vaporization of graphite rods packed with the mixture of yttrium metal and graphite powder (the ratio is 1:15) was conducted under the modified Krätschmer−Huffmann dc-arc discharging method in reactive gas atmosphere with NH_3 as a nitrogen source (atmosphere composition: ammonia 20 mbar and helium 200 mbar). After dc-arc discharging, the soot was preextracted by acetone and then Soxhlet-extracted by CS_2 for 20 h. HPLC isolation running in a Hewlett-Packard instrument (series 1100), a linear combination of two analytical 4.6 × 250 mm Buckyprep (the first step) or Buckyprep-M (the second step) columns (Nacalai Tesque, Japan), was applied with toluene as the eluent (flow rate = 1.6 mL/min; 40 °C). Laser-desorption ionization (LDI) time-of-flight mass spectra were measured using Biflex III system (Bruker, Germany) without matrix.

Details of Computations. Optimization of the molecular structure of all species reported in this work was performed using PBE functional[48] and TZ2P-quality basis set (full-electron {6,3,2}/(11s,6p,2d) for C and N atoms, and SBK-type effective core potential for Y atoms with {5,5,4}/(9s,9p,8d) valence part) implemented in the PRIRODA package.[49,50] This basis set is abbreviated in the manuscript as "TZ2P". The code employed expansion of the electron density in an auxiliary basis set to accelerate evaluation of the Coulomb and exchange-correlation terms.[49]

For the topological analysis, the electron density of EMFs was calculated at the B3LYP level with the use of Firefly/PC GAMESS package[51] and 6-311G* basis set for C and N atoms and full-electron TZVP {8,6,5}/(19s,14p,9d) basis set for Y atoms.[52] QTAIM (quantum theory of atoms in molecules) analysis of the electron densities was performed with the use of AIMAll code (version 08.05.04, http://aim.tkgristmill.com). The PROMEGA algorithm was used for the integration because the less time-demanding PROAIM algorithm often failed, especially for the yttrium atoms and the carbon atoms to which they are bonded. ELF analysis was performed using the TopMoD 09 suite.[53] In view of the ambiguities of the ELF definition for the open shell systems and similar bonding situation in $Y_3@C_{80}$ and $Y_3@C_{80}^+$, ELF calculations were performed for the closed shell $Y_3@C_{80}^+$ cation.

Plane-wave DFT calculations were performed using the CPMD code,[54] PBE functional, and Trouiller−Martins norm-conserving pseudopotentials for Y and C atoms.[55] $Y_3@C_{80}$ molecule was placed inside the center of the simple-cubic cell with the cell parameter of 26.4 Å (50 Bohr), and the plane-wave cutoff of 100 Ry was used throughout the calculations.

Velocity Verlet algorithm with the time step 1.5 fs was used in Born−Oppenheimer molecular dynamics (BOMD) calculations. The energies and gradients were computed with PRIRODA using PBE functional and above-mentioned basis set for the nitrogen and yttrium atoms, while the basis set for the carbon atoms was reduced by one polarization d function. Molecules were first equilibrated at 300 K for 0.6 ps by rescaling velocities when the deviation of the instant temperature from 300 K exceeded 20 K. Then, the trajectory was followed without a thermostat (*i.e.*, in microcanonical ensemble).

Visualization of the computational results was done using ChemCraft[56] (Figures 2−4), Molekel[57] (Figure 5a−f), VESTA[58] (Figure 5g,h), and VMD[59] (Figure 6a,b).

Acknowledgment. A.A.P. acknowledges AvH foundation for financial support and "Chebyshev SKIF-MSU" supercomputer in Moscow State University for a computer time. Technical assistance of U. Nitzsche with local computer resources in IFW is highly appreciated. L.Z. appreciates the financial support from Chinese Scholar Council. Suggestions of the anonymous reviewers to discuss SAMOs and electron affinities in the context of this work are highly appreciated.

Supporting Information Available: Isotopic distribution for $Y_3@C_{80}$, DFT-computed EA and IP values for a series of $Y_3N@C_{2n}$ molecules, $Y_3@C_{80}$, $Y_2C_2@C_{82}$, $Y@C_{82}$, and selected empty higher fullerenes; relative energies of $Y_3@C_{98}$ and $Y_3C_2@C_{96}$ isomers; additional details of molecular dynamics simulations; MOs of $Y_3@C_{80}$ obtained in the plane-wave calculations. This material is available free of charge *via* the Internet at http://pubs.acs.org.

REFERENCES AND NOTES

1. Shinohara, H. Endohedral Metallofullerenes. *Rep. Prog. Phys.* **2000**, *63*, 843–892.
2. Akasaka, T.; Nagase, H. *Endofullerenes: A New Family of Carbon Clusters*; Kluwer: Dordrecht, The Netherlands, 2002.
3. Stevenson, S.; Mackey, M. A.; Stuart, M. A.; Phillips, J. P.; Easterling, M. L.; Chancellor, C. J.; Olmstead, M. M.; Balch, A. L. A Distorted Tetrahedral Metal Oxide Cluster Inside an Icosahedral Carbon Cage. Synthesis, Isolation, and Structural Characterization of $Sc_4(\mu^3\text{-}O)_2@I_h\text{-}C_{80}$. *J. Am. Chem. Soc.* **2008**, *130*, 11844–11845.
4. Valencia, R.; Rodriguez-Fortea, A.; Stevenson, S.; Balch, A. L.; Poblet, J. M. Electronic Structures of Scandium Oxide Endohedral Metallofullerenes, $Sc_4(\mu^3\text{-}O)_n@I_h\text{-}C_{80}$ (n = 2, 3). *Inorg. Chem.* **2009**, *48*, 5957–5961.
5. Stevenson, S.; Rice, G.; Glass, T.; Harich, K.; Cromer, F.; Jordan, M. R.; Craft, J.; Hadju, E.; Bible, R.; Olmstead, M. M.; Maitra, K.; Fisher, A. J.; Balch, A. L.; Dorn, H. C. Small-Bandgap Endohedral Metallofullerenes in High Yield and Purity. *Nature* **1999**, *401*, 55–57.
6. Stevenson, S.; Fowler, P. W.; Heine, T.; Duchamp, J. C.; Rice, G.; Glass, T.; Harich, K.; Hajdu, E.; Bible, R.; Dorn, H. C. A Stable Non-Classical Metallofullerene Family. *Nature* **2000**, *408*, 427–428.
7. Dunsch, L.; Yang, S. Metal Nitride Cluster Fullerenes: Their Current State and Future Prospects. *Small* **2007**, *3*, 1298–1320.
8. Dunsch, L.; Krause, M.; Noack, J.; Georgi, P. Endohedral Nitride Cluster Fullerenes—Formation and Spectroscopic Analysis of $L_{3-x}M_xN@C_{2n}$ ($0 \le x \le 3$; n = 39, 40). *J. Phys. Chem. Solids* **2004**, *65*, 309–315.
9. Krause, M.; Wong, J.; Dunsch, L. Expanding the World of Endohedral Fullerenes—The $Tm_3N@C_{2n}$ ($39 \le n \le 43$) Clusterfullerene Family. *Chem.—Eur. J.* **2005**, *11*, 706–711.
10. Yang, S. F.; Dunsch, L. A Large Family of Dysprosium-Based Trimetallic Nitride Endohedral Fullerenes: $Dy_3N@C_{2n}$ ($39 \le n \le 44$). *J. Phys. Chem. B* **2005**, *109*, 12320–12328.
11. Chaur, M. N.; Melin, F.; Elliott, B.; Athans, A. J.; Walker, K.; Holloway, B. C.; Echegoyen, L. $Gd_3N@C_{2n}$ (n = 40, 42, and 44): Remarkably Low HOMO-LUMO Gap and Unusual Electrochemical Reversibility of $Gd_3N@C_{88}$. *J. Am. Chem. Soc.* **2007**, *129*, 14826–14829.
12. Melin, F.; Chaur, M. N.; Engmann, S.; Elliott, B.; Kumbhar, A.; Athans, A. J.; Echegoyen, L. The Large $Nd_3N@C_{2n}$ ($40 \le 2n \le 49$) Cluster Fullerene Family: Preferential Templating of a C_{88} Cage by a Trimetallic Nitride Cluster. *Angew. Chem., Int. Ed.* **2007**, *46*, 9032–9035.
13. Chaur, M. N.; Melin, F.; Ashby, J.; Kumbhar, A.; Rao, A. M.; Echegoyen, L. Lanthanum Nitride Endohedral Fullerenes $La_3N@C_{2n}$ ($43 < n < 55$): Preferential Formation of $La_3N@C_{96}$. *Chem.—Eur. J.* **2008**, *14*, 8213–8219.
14. Krause, M.; Ziegs, F.; Popov, A. A.; Dunsch, L. Entrapped Bonded Hydrogen in a Fullerene: The Five-Atom Cluster Sc_3CH in C_{80}. *ChemPhysChem* **2007**, *8*, 537–540.
15. Wang, C. R.; Kai, T.; Tomiyama, T.; Yoshida, T.; Kobayashi, Y.; Nishibori, E.; Takata, M.; Sakata, M.; Shinohara, H. A Scandium Carbide Endohedral Metallofullerene: $(Sc_2C_2)@C_{84}$. *Angew. Chem., Int. Ed.* **2001**, *40*, 397–399.
16. Shi, Z. Q.; Wu, X.; Wang, C. R.; Lu, X.; Shinohara, H. Isolation and Characterization of $Sc_2C_2@C_{68}$: A Metal-Carbide Endofullerene with a Non-IPR Carbon Cage. *Angew. Chem., Int. Ed.* **2006**, *45*, 2107–2111.
17. Iiduka, Y.; Wakahara, T.; Nakajima, K.; Tsuchiya, T.; Nakahodo, T.; Maeda, Y.; Akasaka, T.; Mizorogi, N.; Nagase, S. ^{13}C NMR Spectroscopic Study of Scandium Dimetallofullerene, $Sc_2@C_{84}$ *vs* $Sc_2C_2@C_{82}$. *Chem. Commun.* **2006**, 2057–2059.
18. Iiduka, Y.; Wakahara, T.; Nakahodo, T.; Tsuchiya, T.; Sakuraba, A.; Maeda, Y.; Akasaka, T.; Yoza, K.; Horn, E.; Kato, T.; Liu, M. T. H.; Mizorogi, N.; Kobayashi, K.; Nagase, S. Structural Determination of Metallofullerene Sc_3C_{82} Revisited: A Surprising Finding. *J. Am. Chem. Soc.* **2005**, *127*, 12500–12501.

19. Yang, H.; Lu, C.; Liu, Z.; Jin, H.; Che, Y.; Olmstead, M. M.; Balch, A. L. Detection of a Family of Gadolinium-Containing Endohedral Fullerenes and the Isolation and Crystallographic Characterization of One Member as a Metal-Carbide Encapsulated Inside a Large Fullerene Cage. *J. Am. Chem. Soc.* **2008**, *130*, 17296–17300.
20. Inoue, T.; Tomiyama, T.; Sugai, T.; Okazaki, T.; Suematsu, T.; Fujii, N.; Utsumi, H.; Nojima, K.; Shinohara, H. Trapping a C_2 Radical in Endohedral Metallofullerenes: Synthesis and Structures of $(Y_2C_2)@C_{82}$ (Isomers I, II, and III). *J. Phys. Chem. B* **2004**, *108*, 7573–7579.
21. Tagmatarchis, N.; Aslanis, E.; Prassides, K.; Shinohara, H. Mono-, Di- and Trierbium Endohedral Metallofullerenes: Production, Separation, Isolation, and Spectroscopic Study. *Chem. Mater.* **2001**, *13*, 2374–2379.
22. Lian, Y. F.; Shi, Z. J.; Zhou, X. H.; Gu, Z. N. Different Extraction Behaviors between Divalent and Trivalent Endohedral Metallofullerenes. *Chem. Mater.* **2004**, *16*, 1704–1714.
23. Yang, S. F.; Dunsch, L. Di- and Tridysprosium Endohedral Metallofullerenes with Cages from C_{94} to C_{100}. *Angew. Chem., Int. Ed.* **2006**, *45*, 1299–1302.
24. Shinohara, H.; Sato, H.; Ohkohchi, M.; Ando, Y.; Kodama, T.; Shida, T.; Kato, T.; Saito, Y. Encapsulation of a Scandium Trimer in C_{82}. *Nature* **1992**, *357*, 52–54.
25. Yang, D.-S.; Zgierski, M. Z.; Hackett, P. A. Bonding and Structure of Y_3C_2 and $Y_3C_2^+$. *J. Chem. Phys.* **1998**, *108*, 3591–3597.
26. Popov, A. A.; Krause, M.; Yang, S. F.; Wong, J.; Dunsch, L. C_{78} Cage Isomerism Defined by Trimetallic Nitride Cluster Size: A Computational and Vibrational Spectroscopic Study. *J. Phys. Chem. B* **2007**, *111*, 3363–3369.
27. Popov, A. A.; Dunsch, L. The Bonding Situation in Endohedral Metallofullerenes as Studied by Quantum Theory of Atoms in Molecules (QTAIM). *Chem.—Eur. J.* **2009**, *15*, 9707–9729.
28. Popov, A. A. Metal-Cage Bonding, Molecular Structures and Vibrational Spectra of Endohedral Fullerenes: Bridging Experiment and Theory. *J. Comput. Theor. Nanosci.* **2009**, *6*, 292–317.
29. Kobayashi, K.; Nagase, S. Theoretical Study of Structures and Dynamic Properties of $Sc_3@C_{82}$. *Chem. Phys. Lett.* **1999**, *313*, 45–51.
30. Chaur, M. N.; Athans, A. J.; Echegoyen, L. Metallic Nitride Endohedral Fullerenes: Synthesis and Electrochemical Properties. *Tetrahedron* **2008**, *64*, 11387–11393.
31. Chaur, M. N.; Melin, F.; Elliott, B.; Kumbhar, A.; Athans, A. J.; Echegoyen, L. New $M_3N@C_{2n}$ Endohedral Metallofullerene Families (M = Nd, Pr, Ce; $n = 40-53$): Expanding the Preferential Templating of the C_{88} Cage and Approaching the C_{96} Cage. *Chem.—Eur. J.* **2008**, *14*, 4594–4599.
32. Fu, W.; Xu, L.; Azurmendi, H.; Ge, J.; Fuhrer, T.; Zuo, T.; Reid, J.; Shu, C.; Harich, K.; Dorn, H. C. ^{89}Y and ^{13}C NMR Cluster and Carbon Cage Studies of an Yttrium Metallofullerene Family, $Y_3N@C_{2n}$ ($n = 40-43$). *J. Am. Chem. Soc.* **2009**, *131*, 11762–11769.
33. Zuo, T.; Xu, L.; Beavers, C. M.; Olmstead, M. M.; Fu, W.; Crawford, T. D.; Balch, A. L.; Dorn, H. C. $M_2@C_{79}N$ (M = Y, Tb): Isolation and Characterization of Stable Endohedral Metallofullerenes Exhibiting M···M Bonding Interactions Inside Aza[80]Fullerene Cages. *J. Am. Chem. Soc.* **2008**, *130*, 12992–12997.
34. Popov, A. A.; Dunsch, L. Structure, Stability, and Cluster-Cage Interactions in Nitride Clusterfullerenes $M_3N@C_{2n}$ (M = Sc, Y; $2n = 68-98$): A Density Functional Theory Study. *J. Am. Chem. Soc.* **2007**, *129*, 11835–11849.
35. McAdon, M. H.; Goddard, W. A., III. New Concepts of Metallic Bonding Based on Valence-Bond Ideas. *Phys. Rev. Lett.* **1985**, *55*, 2563–2566.
36. Bader, R. F. W. *Atoms in Molecules: A Quantum Theory*; Oxford University Press: Oxford, 1990.
37. Silvi, B.; Savin, A. Classification of Chemical Bonds Based on Topological Analysis of Electron Localization Function. *Nature* **1994**, *371*, 683–686.
38. Savin, A.; Nesper, R.; Wenger, S.; Fassler, T. F. ELF: The Electron Localization Function. *Angew. Chem., Int. Ed.* **1997**, *36*, 1808–1832.
39. Kohout, M.; Wagner, F. R.; Grin, Y. Electron Localization Function for Transition-Metal Compounds. *Theor. Chem. Acc.* **2002**, *108*, 150–156.
40. Pendas, A. M.; Blanco, M. A.; Costales, A.; Sanchez, P. M.; Luana, V. Non-Nuclear Maxima of the Electron Density. *Phys. Rev. Lett.* **1999**, *83*, 1930–1933.
41. Gatti, C.; Fantucci, P.; Pacchioni, G. Charge Density Topological Study of Bonding in Lithium Clusters. Part I: Planar Li_n Clusters ($n = 4, 5, 6$). *Theor. Chim. Acta* **1987**, *72*, 433–458.
42. Feng, M.; Zhao, J.; Petek, H. Atomlike, Hollow-Core-Bound Molecular Orbitals of C_{60}. *Science* **2008**, *320*, 359–362.
43. Zhao, J.; Feng, M.; Yang, J.; Petek, H. The Superatom States of Fullerenes and Their Hybridization into the Nearly Free Electron Bands of Fullerites. *ACS Nano* **2009**, *3*, 853–864.
44. Kua, J.; Goddard, W. A., III. Chemisorption of Organics on Platinum. 1. The Interstitial Electron Model. *J. Phys. Chem. B* **1998**, *102*, 9481–9491.
45. Taubert, S.; Straka, M.; Pennanen, T. O.; Sundholm, D.; Vaara, J. Dynamics and Magnetic Resonance Properties of $Sc_3C_2@C_{80}$ and Its Monoanion. *Phys. Chem. Chem. Phys.* **2008**, *10*, 7158–7168.
46. Heine, T.; Vietze, K.; Seifert, G. ^{13}C NMR Fingerprint Characterizes Long Time-Scale Structure of $Sc_3N@C_{80}$ Endohedral Fullerene. *Magn. Reson. Chem.* **2004**, *42*, S199–S201.
47. Yang, S.; Popov, A. A.; Dunsch, L. Carbon Pyramidalization in Fullerene Cages Induced by the Endohedral Cluster: Non-Scandium Mixed Metal Nitride Clusterfullerenes. *Angew. Chem., Int. Ed.* **2008**, *47*, 8196–8200.
48. Perdew, J. P.; Burke, K.; Ernzerhof, M. *Phys. Rev. Lett.* **1996**, *77*, 3865–3868.
49. Laikov, D. N. Fast Evaluation of Density Functional Exchange-Correlation Terms Using the Expansion of the Density in Auxiliary Basis Sets. *Chem. Phys. Lett.* **1997**, *281*, 151–156.
50. Laikov, D. N.; Ustynyuk, Y. A. Priroda-04: A Quantum-Chemical Program Suite. New Possibilities in the Study of Molecular Systems with the Application of Parallel Computing. *Russ. Chem. Bull., Int. Ed.* **2004**, *54*, 820–826.
51. Granovsky, A. A. *PC Gamess/Firefly*, version 7.1.C; http://classic.chem.msu.su/gran/gamess/Index.html, 2008.
52. Ahlrichs, R.; May, K. Contracted All-Electron Gaussian Basis Sets for Atoms Rb to Xe. *Phys. Chem. Chem. Phys.* **2000**, *2*, 943–945.
53. Noury, S.; Krokidis, X.; Fuster, F.; Silvi, B. Topmod. *Comput. Chem.* **1999**, *23*, 597–604.
54. *CPMD*, Copyright IBM Corp. 1990−2008; Copyright MPI Für Festkörperforschung Stuttgart 1997−2001; http://www.cpmd.org, 2008.
55. Troullier, N.; Martins, J. L. Efficient Pseudopotentials for Plane-Wave Calculations. *Phys. Rev. B* **1991**, *43*, 1993–2006.
56. Zhurko, G. A. *Chemcraft*, version 1.5; http://www.chemcraftprog.com.
57. Flukiger, P.; Luthi, H. P.; Portmann, S.; Weber, J. *Molekel 4.3*, Swiss Center for Scientific Computing; http://www.cscs.ch/molkel, 2002.
58. Momma, K.; Izumi, F. VESTA: A Three-Dimensional Visualization System for Electronic and Structural Analysis. *J. Appl. Crystallogr.* **2008**, *41*, 653–658.
59. Humphrey, W.; Dalke, A.; Schulten, K. VMD—Visual Molecular Dynamics. *J. Mol. Graphics* **1996**, *14*, 33–38.